

GW+ U real-space Green's function calculations of x-ray spectra

Towfiq Ahmed, J. J. Kas, and J. J. Rehr

Dept. of Physics, Univ. of Washington Seattle, WA 98195

(Dated: July 12, 2011)

Abstract

The Hubbard model is implemented in real-space Green's function calculations of x-ray spectra using an effective self-energy adapted from the LSDA+ U method of Anisimov *et al.* This self-energy consists of an energy-dependent many-pole approximation to the GW self-energy with an additive correction due to on-site Coulomb repulsion among the partially filled localized-electron states. This leads to a GW+ U approach which provides an efficient procedure to account for local correlation effects on x-ray spectra. Results are presented for the spin and angular momentum projected density of states of MnO, NiO, and $\text{La}_{2-x}\text{Sr}_x\text{CuO}_4$ (LSCO), for the K-edge x-ray spectra of O atoms in MnO and NiO, and the unoccupied electronic states and O K-edge spectra of undoped LSCO. The method is found to yield reasonable agreement with experiment.

PACS numbers: 78.70.Dm, 71.10.Fd, 71.10.-w, 71.15.Qe

Keywords: Hubbard model, RSGF, LSCO, GW+ U , K-edge XANES

I. INTRODUCTION

Density functional theory (DFT) together with quasi-particle corrections has been remarkably successful in describing the electronic structure and band-gaps of weakly interacting systems. For such systems, these quasi-particle corrections are often well described in terms of Hedin's GW self-energy^{1,2} (where G refers to the one-particle Green's function and W the screened Coulomb interaction). On the other hand, the GW approach is generally inadequate to describe the band gap and other electronic properties in materials with well localized $3d$ or $4f$ electrons.³ On the other hand, the strong local Coulomb interactions in these systems can often be approximated using a Hubbard-model,³ in which the on-site electron-electron repulsion is represented by spin- and orbital-occupancy dependent "Hubbard parameters" U and J . Combining the local spin density approximation (LSDA) of DFT with the Hubbard model leads to the LSDA+ U method. In practice, the Hubbard correction is added to the original Kohn-Sham LSDA Hamiltonian while an approximate mean-field term is subtracted to avoid double-counting.⁴ In order to calculate the excited state properties and x-ray spectra of correlated systems, it is desirable to go beyond LSDA+ U and incorporate energy dependent self-energy effects in terms of Hedin GW self-energy. This is the approach adopted here, which we refer to as the GW+ U method. A related approach has been proposed by Jiang *et al*, where an accurate GW self-energy is calculated starting with LSDA+ U . Besides providing an improved screening model, their approach correctly predicts the band-gap in several d and f electron systems.^{5,6} In another prescription, Bansil *et al* developed a self-consistent GW+ U scheme based on the tight-binding approximation and a single-band Hubbard model.^{7,8} Their method is found to qualitatively explain several pre-edge spectral features in high T_c cuprates.^{9,10} Here we add Hubbard correction terms to an approximate many-pole GW self-energy¹¹ in a single-step approach, although formally such corrections could be incorporated within a self-consistent GW framework.⁴ The implementation of our approach within the real-space Green's function (RSGF) formalism simplifies the calculation compared to conventional LSDA/GW+ U methods, and is one of the primary goals of this paper. With the aid of this extension, we investigate the effects of correlated d -electron states on the angular momentum projected density of states (IDOS), and the excited state spectra including x-ray absorption spectra (XAS) and x-ray emission spectra (XES) of a number of materials. As in other codes, e.g., WIEN2K¹² and SPRKKR,¹³

the Hubbard parameters are here treated as fitting parameters.

Our RSGF/GW+ U method is tested on several d -electron systems including MnO, NiO and the undoped high T_c cuprate $\text{La}_{2-x}\text{Sr}_x\text{CuO}_4$ (LSCO). In these materials, the electronic structure and band gaps are strongly influenced by U , the charge-transfer energy Δ , and the one-electron band-width W . Related calculations for MnO and NiO have also been carried out using a combined GW/LDA+ U approach by Jiang *et al.*⁵ Treatments of Ti oxide compounds using LDA+ U within the multiple scattering formalism have also been carried out by Krüger.¹⁴ We find that our approach yields reasonable agreement with bulk-sensitive probes such as XES and XAS which are used to measure band gaps between occupied and unoccupied states.¹⁵

II. THEORY AND METHODOLOGY

In this Section we describe our implementation of the GW+ U method as an extension of the real-space Green's function (RSGF) multiple-scattering formalism.^{16,17} Our implementation follows the strategy used in the FEFF9 code and thus permits calculations of both electronic structure and x-ray spectra that can account for local atomic-correlation effects. Hartree atomic units ($e = \hbar = m = 1$) are implicit unless otherwise specified.

A. RSGF Method

We begin with a brief outline of the RSGF formalism used in this work. In this approach physical quantities of interest are expressed in terms of the local quasi-particle Green's function $G(\mathbf{r}, \mathbf{r}', E)$. For example, the physical quantity measured in XAS for photons of polarization $\hat{\epsilon}$ and energy ω is the x-ray absorption coefficient $\mu(\omega)$,

$$\mu(\omega) \propto -\frac{2}{\pi} \text{Im} \langle \phi_c | \hat{\epsilon} \cdot \mathbf{r} G(\mathbf{r}, \mathbf{r}', \omega + E_c) \hat{\epsilon} \cdot \mathbf{r}' | \phi_c \rangle, \quad (1)$$

where E_c is the core electron energy and $|\phi_c\rangle$ is the core state wave function. The FEFF9 code also calculates closely related quantities such as the spin and angular momentum projected density of states (l DOS) $\rho_{l\sigma}^{(n)}(E)$ at site n ,

$$\rho_{l\sigma}^{(n)}(E) = -\frac{1}{\pi} \text{Im} \sum_m \int_0^{R_n} G_{L,L}^{\sigma,\sigma}(r, r, E) r^2 dr, \quad (2)$$

where R_n is the Norman radius around the n^{th} atom,¹⁸ which is analogous to the Wigner-Seitz radius of neutral spheres, and the factor 2 accounts for spin degeneracy. The coefficients $G_{L,L'}^{\sigma,\sigma'}$ characterize the expansion of the Green's function $G(\mathbf{r}, \mathbf{r}', E)$ in spherical harmonics,

$$G(\mathbf{r}, \mathbf{r}', E) = \sum_{L,L',\sigma} Y_L(\hat{\mathbf{r}}) G_{L,L'}^{\sigma,\sigma}(r, r', E) Y_{L'}^*(\hat{\mathbf{r}}'), \quad (3)$$

where $L = (l, m)$ denotes both orbital and azimuthal quantum numbers. In these formulae, the quasi-particle Green's function for an excited electron at energy E is given formally (matrix-indices suppressed) by

$$G(E) = [E - H - \Sigma(E)]^{-1}, \quad (4)$$

where H is the independent-particle Hamiltonian

$$H = \frac{p^2}{2} + V, \quad (5)$$

and V is the Hartree-potential. For convenience in our calculations, the Hamiltonian is re-expressed in terms of a Kohn-Sham Hamiltonian $H^{KS} = H + V_{xc}$ where V_{xc} is a ground state exchange-correlation¹⁹ functional, and the self-energy is replaced by a modified self-energy $\Sigma(E) - V_{xc}$ which is set to zero at the Fermi-energy $E = E_F$. In this work we use the von Barth-Hedin LSDA functional $V_{xc}[n(\mathbf{r}), m(\mathbf{r})]$,¹⁹ where $n(\mathbf{r}) = n_\uparrow + n_\downarrow$ is the total electron density and $m(\mathbf{r}) = n_\uparrow - n_\downarrow$ is the spin polarization density. In practice, it is useful to decompose the total Green's function $G(E)$ as

$$G(E) = G^c(E) + G^{sc}(E), \quad (6)$$

where $G^c(E)$ is the contribution from the central (absorbing) atom and $G^{sc}(E)$ is the scattering part. Full multiple scattering (FMS) calculations can be carried out by matrix inversion, i.e., with $G = [1 - G^0 T]^{-1} G^0$, where G^0 is the bare propagator and T is the scattering T-matrix, which are represented in an angular-momentum and site basis: $G^0 = G_{nL,n'L'}^0(E)[1 - \delta_{n,n'}]$ and $T = t_{nL}^\sigma \delta_{l,l'} \delta_{m,m'} \delta_{n,n'} \delta_{\sigma,\sigma'}$. Finally, t_{nL}^σ is the single site scattering matrix, which is related to the single site phase shifts, i.e.,

$$t_{nL}^\sigma = \exp(i\delta_{nL}^\sigma) \sin(\delta_{nL}^\sigma).$$

Within the spherical muffin-tin approximation, $G^c(E)$ can be expanded in terms of the regular $R_L(\mathbf{r}, E)$ and irregular $H_L(\mathbf{r}, E)$ solutions of the single site Schrödinger equation.²⁰

In the FEFF code a typical calculation of the electronic structure (ground or excited state) starts with a self-consistent calculation of the electron density and Kohn-Sham potentials.¹⁸ Once the self-consistent potential is obtained, the Green's function is constructed and used to calculate XAS and other quantities of interest. Of particular interest in this paper is the local spin-dependent density matrix for the n -th site

$$n_{nlm,nlm'}^{\sigma\sigma'} = -\frac{1}{\pi} \int^{E_F} dE \int_{cell} \text{Im} G_{nlm,nlm'}^{\sigma\sigma'}(\mathbf{r}, \mathbf{r}, E) d^3r, \quad (7)$$

where the n denotes the cell defined by the Norman sphere centered about the n^{th} atom, \mathbf{r}, \mathbf{r}' are relative to the center of the cell R_n , and σ is the spin-index, and we explicitly designate the azimuthal quantum numbers m and m' . For a more detailed description of the multiple scattering RSGF method see Refs. [20,21].

B. GW+ U Self-energy

Quasi-particle effects are key to an accurate treatment of excited state spectra,¹⁶ and hence we need a good approximation for the electron self-energy. Current approximations for the self-energy typically begin with Hedin's GW approximation (GWA),² which is formally given by

$$\Sigma = iGW \quad (8)$$

where G is the one electron Green's function, $W = \epsilon^{-1}v$, is the screened-Coulomb interaction, and v the bare-Coulomb interaction. The FEFF9 code uses several approximations for the self-energy with the aim of providing efficient calculations of the energy dependent shift and broadening of spectral features. The default, which is appropriate at high energies, is the Hedin-Lundqvist plasmon-pole model,^{2,22} based on the electron gas and a single-pole approximation to the dielectric function. An extension which improves the self energy at low energies is a many-pole model, where the the dielectric function is represented as a weighted sum of poles matched to calculations of the loss function in the long wavelength limit.¹¹ Although these models significantly improve quasi-particle calculations of unoccupied states, they do not necessarily obtain accurate band-gap corrections. In our implementation of GW+ U , an energy, spin and orbital dependent total potential is constructed that incorporates the GW plasmon-pole or many-pole self energy $\Sigma(E)$ and the Hubbard correction V_{lm}^U , with parameters chosen to obtain the correct gap. Although such a construction can be

done using self-consistent methods,²³ here we use only a single-step calculation. Thus we define our total potential as

$$V(\mathbf{r}, E) = V_{\sigma}^{LSDA}(\mathbf{r}) + \Sigma^{GW}(E) + V_{lm\sigma}^U. \quad (9)$$

The orbital and spin-dependent Hubbard contribution to the potential is calculated as described in the next section.

C. LSDA+ U formalism

Our construction of $V_{lm\sigma}^U(E)$ is adapted from the LSDA+ U approach of Anisimov *et al.*⁴ In their approach one starts with the total energy functional of the system and adds a Hubbard correction to account for the Coulomb interaction between localized, strongly correlated electrons. It is generally assumed²⁴ that a similar mean-field term should exist in LSDA or other DFT approaches which must be subtracted from the energy functional to avoid double counting,

$$\begin{aligned} E^U[n^{\sigma}(\vec{r}), \mathbf{n}^{\sigma}] &= E^{LSDA}[n^{\sigma}(\vec{r})] \\ &+ E^U[\mathbf{n}^{\sigma}] - E_{dc}[\mathbf{n}^{\sigma}], \end{aligned} \quad (10)$$

where $n^{\sigma}(\vec{r})$ is the charge density, \mathbf{n}^{σ} the density matrix, E^U the Hubbard interaction, and E_{dc} the double counting term. The Hubbard term depends on the density matrix $n_{ilm,ilm'}^{\sigma\sigma'}$, and on-site Coulomb interactions between the localized electrons.

As discussed by Albers *et al.*,²⁴ an *ab initio* determination of the Hubbard parameters is not straightforward, since they are sensitive to screening of the Coulomb interaction. Hence, the Hubbard terms are often regarded as fitting parameters while the density matrix is calculated from first-principles to construct the Hubbard potential. This is the approach adopted here. While it may be possible to go beyond this parametrization and calculate the Hubbard terms using approaches such as constrained-LDA^{25,26}, or constrained-RPA,^{27,28}, such estimates are beyond the scope of this paper. For systems where the localized electrons are atomic-like, the density matrix can be approximated²⁹ as

$$n_{mm'}^{\sigma} = n_m^{\sigma} \delta_{mm'}. \quad (11)$$

This spherical approximation is reasonable for many systems including TMOs, and good agreement for the band gap is found when the non-sphericity of d-d interaction as well

as the off-diagonal terms of $n_{mm'}$ are ignored.³ With these approximations, the number of parameters is reduced to only two, namely U and J representing the screened direct and exchange intra-atomic Coulomb interactions, respectively.

The total energy functional can then be written as

$$E = E^{LSDA} + \frac{1}{2} \sum_{m,m',\sigma} U(n_m^\sigma - n^o)(n_{m'}^{-\sigma} - n^o) + \frac{1}{2} \sum_{m,m' \neq m,\sigma} (U - J)(n_m^\sigma - n^o)(n_{m'}^\sigma - n^o). \quad (12)$$

Here the double counting term E_{dc} is represented by n^o where $n^o = n_d/10$ and $n_d = \sum_{m\sigma} n_m^\sigma$. Using $V(\vec{r}) = \delta E / \delta n_\sigma(\vec{r})$, a simplified expression for the total LSDA+ U potential is finally obtained,²⁹ i.e.,

$$V^{LSDA+U}(\vec{r}) = V^{LSDA}(\vec{r}) + V_{lm\sigma}^U, \quad (13)$$

where

$$V_{lm\sigma}^U = U \sum_{m'} (n_{lm'}^{-\sigma} - n_o) + (U - J) \sum_{m' \neq m} (n_{lm'}^\sigma - n_o). \quad (14)$$

Within the spherical approximation, we need only consider the diagonal elements n_{lm}^σ of the density matrix defined in Eq. (7). In a single-step spin-dependent calculation using the von Barth-Hedin LSDA functional, we first obtain n_{lm}^σ . In this prescription, a prior knowledge of spin polarization of i -th atom $m_i = n_i^\uparrow - n_i^\downarrow$ is required. For Mn, Ni, and Cu we used $m = 5, 2$, and 1 correspondingly using Hund's multiplicity rule^{30,31} for free atoms which is often treated as good approximations for such systems.

The occupancy of the spin-up and -down states within the d -orbitals are thus determined in this single-step LSDA approach. Our calculations of spin-orbital occupancies of Mn and Ni d -states using this scheme are listed in Tables I and II. Thus we essentially start with a spin dependent ground state calculation and introduce spin and orbital dependence using Anisimov's prescription of Hubbard model. This LSDA+ U prescription is found to provide good agreement between the theory and experiment for the XAS of the TM compounds investigated here, although the self-consistent LSDA+ U treatment may be more desirable in other cases.

Values for the U and J parameters are taken either from previous work^{3,32} or chosen to fit the experimental band gap. For MnO and NiO, we used $U \approx 4.5$ and 7.5 eV and $J = 0.9$ eV, which are reasonably close to those calculated or discussed by other authors.^{5,32} Using Eqs.

(9) and (14) we then correct our self-consistent quasi-particle (QP) potential and obtain a new potential $V^{GW+U}(\mathbf{r}, E)$ given by

$$V_{\sigma}^{GW+U}(\mathbf{r}, E) = V_{\sigma}^{LSDA}(\mathbf{r}) + \Sigma^{GW}(E) + V_{lm\sigma}^U(E). \quad (15)$$

Then using the GW+ U Hamiltonian above, the wave functions $R_L(\mathbf{r}, E)$ and $H_L(\mathbf{r}, E)$ are recalculated as solutions of the Schrödinger equation inside the muffin-tin spheres with our Hubbard modified potential. The orbital dependent phase shifts $\delta_{lm}^{\sigma}(E)$ are obtained by matching to the free solutions (spherical Bessel functions) at the muffin-tin, and the scattering t -matrices are found.

$$t_{lm}^{\sigma} = \exp(i\delta_{lm}^{\sigma}) \sin(\delta_{lm}^{\sigma}). \quad (16)$$

Finally the multiple-scattering equations are resolved with these t -matrices yielding the the total Green's function $G = G^c + G^{sc}$, which now includes the Hubbard- U correction. With the addition of the state dependent Hubbard correction, the potential of Eq. (15) can correctly account for the well known discontinuity^{29,33} in exact DFT exchange-correlation potentials. However, such a term is absent from the conventional LDA and GGA approaches, rendering them incapable of including such band-gap corrections.

III. RESULTS AND DISCUSSION

A. Transition Metal Oxides

Transition metal oxides (TMOs) such as MnO and NiO are considered to be prototypes of strongly correlated Mott type insulators with localized and partially filled d -electrons at the metal sites. These TMOs have NaCl like crystal structures, (Cubic O_h^5 symmetry, and f_{m3m} space group). Below their respective Néel temperatures, they all exhibit a rhombohedral distortion due to anti-ferromagnetic (AF) ordering, which is also known as exchange anisotropy.³⁴ We examined the effects of such crystal distortions but they had negligible influence on the spectral features of interest here. In the following subsections we present results for the total and angular momentum projected DOS of MnO and NiO for a few values of U . The exchange parameter J is typically much smaller than U and variations were found to be small over the transition metals; thus we used $J = 0.9$ eV for all cases.³

For both compounds, the O K-edge XAS and XES are also calculated and compared with experimental results.

1. MnO

In order to compare with room temperature experiment,¹⁵ we have taken an undistorted MnO crystal with $a = b = c = 4.4316$ Å and $\alpha = \beta = 90.624^\circ$.³⁵ In this paper, we do not consider periodic magnetic effects; however, the single site moments are implicitly taken into account in our GW+ U implementation. In our FMS calculations for MnO, we used a

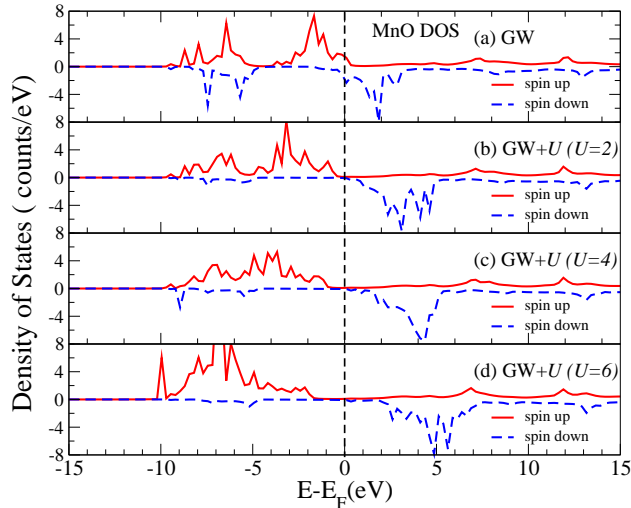


FIG. 1: (Color online) U dependence on total DOS of MnO with spin up (solid red) and spin down (dashed blue) for different values of U : (a) GW ($U=0$), (b) $U = 2.0$ eV, (c) $U = 4.0$ eV and (d) $U = 6.0$ eV; Vertical dashed line is at the Fermi energy.

cluster of 250 atoms, which was adequate to converge the spectrum, and a smaller cluster of 60 atoms for the self-consistent muffin-tin potentials. For this system we calculated the O K edge XES and XAS and the spin and angular momentum projected DOS about the Mn and O sites with and without GW+ U corrections. Fig. 1 shows a comparison of our calculated total ground state spin-resolved DOS of MnO to that calculated with different values of U . While a calculation with a GW self-energy underestimates an insulating gap (dashed blue line in Fig. 1), a gap close to that observed in experiment is obtained using the Hubbard correction $U = 4.6$ eV. When applied to Mn d -states, an upper Hubbard band appears at about +1.5 eV, as seen in Fig. 2(a). The O p -states (Fig. 2(b)) near E_F are strongly

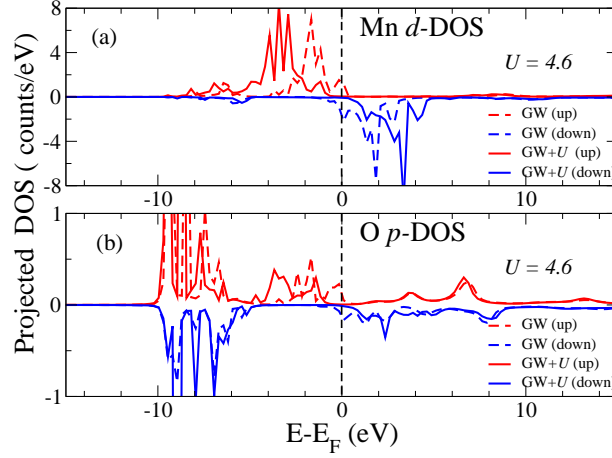


FIG. 2: (Color online) angular momentum projected l -DOS for Mn and O in MnO with GW($U = 0.0$) and GW+ U ($U = 4.6$ eV); Spin up and down DOS are above and below the horizontal axis correspondingly: (a) Mn d -DOS GW(dashed) and GW+ U (solid). (b) similar color and line style correspondence for O p -DOS; Vertical dashed line is at the Fermi energy.

hybridized with Mn d -states (Fig. 2(a)); thus a gap is also seen in the O p -DOS. However, the O p -states around 6-8 eV only hybridize with Mn s - p -states (not shown) and are not affected by the Hubbard correction. In Table (I) we present the spin-orbital occupancies of the localized Mn d -states and the corresponding Hubbard correction for $U = 4.6$ and $J = 0.9$ eV.

TABLE I: Mn d -state parameters ($U = 4.6$; $J = 0.9$ eV)

l	m	n_{lm}	n_{lm}^{\uparrow}	n_{lm}^{\downarrow}	V_{lm}^{\uparrow} (eV)	V_{lm}^{\downarrow} (eV)
2	0	1.02	0.90	0.12	-1.82	1.61
2	± 1	0.97	0.84	0.13	-1.56	1.55
2	± 2	0.95	0.83	0.12	-1.52	1.63

Bulk sensitive XES and XAS for TM oxides often provide a good assessment of the band gap in insulators.¹⁵ In Fig. 3 we compare our GW+ U calculation of the O K-edge XAS and XES with experiment.¹⁵ Fig. 3 shows the result of our spin resolved FMS calculation obtained with both Hubbard and GW self-energy corrections (b) compared to results with no

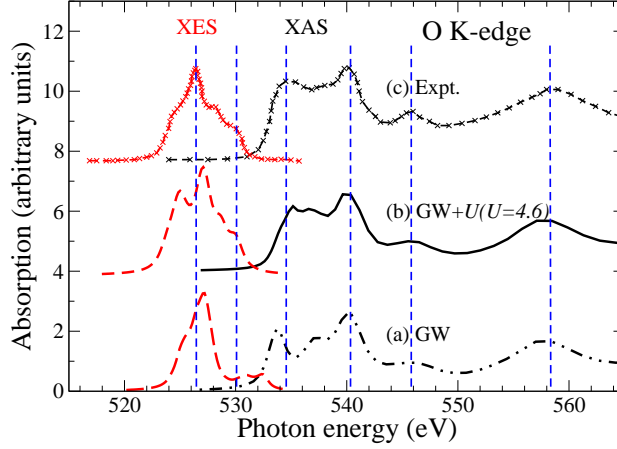


FIG. 3: (Color online) O K-edge XAS (black) and XES (red) in MnO. (a) QP FEFF calculation using GW plasmon-pole self-energy, (b) GW+ U ($U = 4.6$), and (c) experiment.¹⁵ The vertical dashed lines are a guide to the eye.

Hubbard correction (a) and experiment (c). The XAS calculation was done in the presence of a screened core-hole at the absorbing O atom while for XES no core-hole was included; these approximations are consistent with the final-state- and initial-state rules for XAS and XES respectively. Our Hubbard corrected self-energy blue shifts the first excitation at around 534 eV, while the rest of the unoccupied states, including the main peak at 540 eV, are unchanged. In XES, the highest occupied state moves down by 3 eV which is now on the other side of the second vertical dashed line in Fig. 3. These distinct, opposite shifts of the highest occupied and first unoccupied states are due to the strong hybridization of O p -states with the localized Mn d states. This can also be identified in Fig. 2(b) as the lower and upper Hubbard bands (UHB) at around -2 and 2 eV.

2. NiO

In order to compare with room-temperature experiments¹⁵ we have accounted for the rhombohedral distortion along the $[111]$ direction.^{36,37} Our methods for calculating electronic structures of NiO are similar to those for MnO, except for the input NiO crystal structure, where we have used a slightly distorted crystal with $a = b = 4.168$ Å, $c = 4.166$ Å, and $\alpha = \beta = 90.055^\circ$, $\gamma = 90.082^\circ$. With the Hubbard correction, the best agreement with the

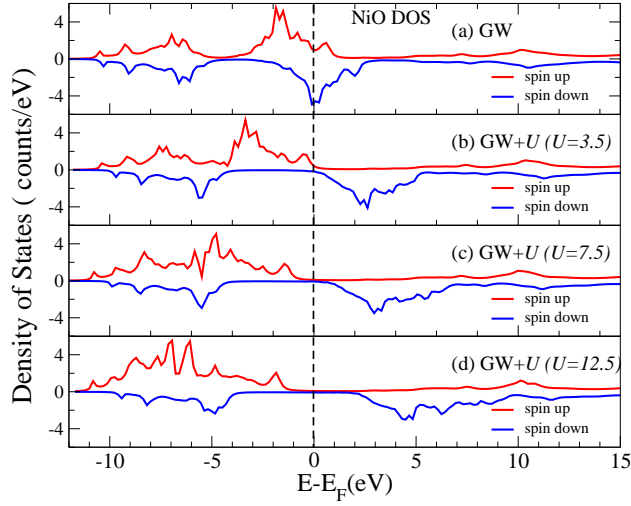


FIG. 4: (Color online) U dependence on total DOS of NiO with spin up (solid red) and spin down (dashed blue) for different values of U : (a) GW ($U=0$), (b) $U = 3.5$ eV, (c) $U = 7.5$ eV and (d) $U = 12.5$ eV; Vertical dashed line is at the Fermi energy.

experimental XAS was again obtained with $U = 7.5$ eV. Fig. 4 and Fig. 5 show the gap opening in the spin projected total DOS of NiO for higher values of U . The O p -states in NiO are also strongly hybridized with localized Ni d -states as in MnO. The spin-orbital occupancies and corresponding Hubbard potential for the Ni d -states are listed in Table II.

TABLE II: Ni d -state parameters ($U = 7.5$ eV; $J = 0.9$)

l	m	n_{lm}	n_{lm}^{\uparrow}	n_{lm}^{\downarrow}	V_{lm}^{\uparrow} (eV)	V_{lm}^{\downarrow} (eV)
2	0	1.22	0.97	0.25	-2.75	3.74
2	± 1	1.64	0.96	0.68	-2.53	1.88
2	± 2	1.44	0.97	0.47	-2.63	2.48

Our GW plasmon-pole calculation in Fig. 6(a) exhibits considerable overlap between the O K-edge XAS and XES spectra, due to the underestimated insulating gap. However, the introduction of the Hubbard interaction ($U = 7.5$ eV) increases the gap, causing the pre-peaks of both the XAS and XES to split further apart, as shown in Fig. 6(b). For comparison, we also show a WIEN2K LDA+ U calculation in Fig. 6(c) for the O K-edge EELS in NiO.³⁸

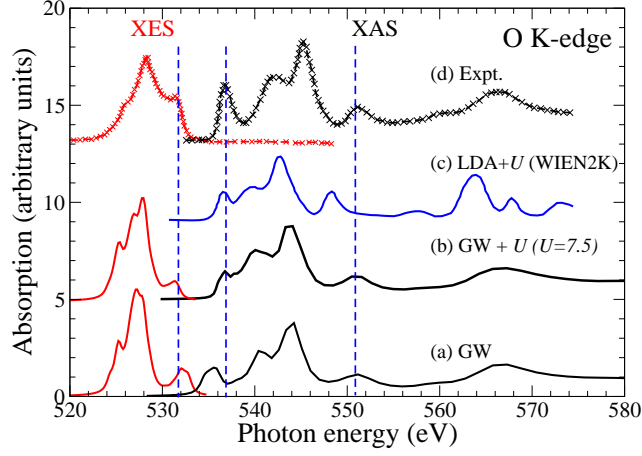


FIG. 6: (Color online) NiO O K-edge XAS (black) and XES (red) experiment vs theory: (a) FEFW GW+ U plasmon-pole (PP) self-energy; (b) FEFW GW+ U with Hubbard correction $U = 7.5$ eV; (c) GW+ U calculation³⁸ for O 1s EELS using WIEN2K; and (d) Experiment.¹⁵ The vertical dashed lines are a guide to the eye.

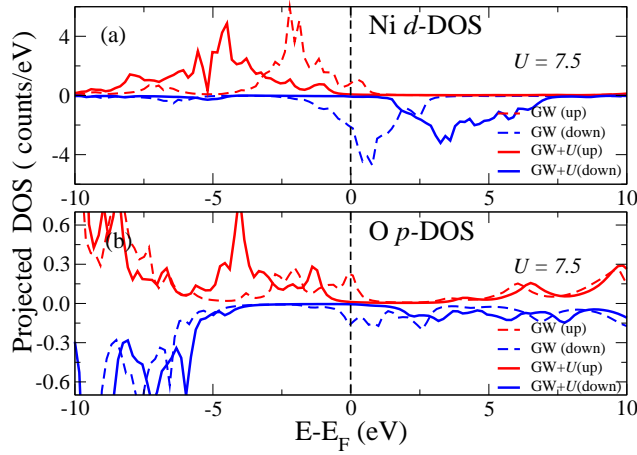


FIG. 5: (Color online) angular momentum projected l -DOS for Ni and O in NiO with GW($U = 0.0$) and GW+ U ($U = 7.5$ eV); Spin up and down DOS are above and below the horizontal axis correspondingly: (a) Ni d -DOS GW(dashed) and GW+ U (solid). (b) similar color and line style correspondence for O p -DOS; Vertical dashed line is at the Fermi energy.

Aligning the first peak of this calculation with experiment [Fig. 6(d)], we observe an un-

derestimation of the high energy peaks at around 544 eV. These peaks can be attributed to O p -states which are strongly hybridized with Ni s - and p -states. Similar behavior has been found in NiO,^{5,39} and other TM compounds.^{38,40} We attempted to improve these results by using a more accurate GW many-pole self-energy¹¹ for NiO, while applying the Hubbard correction to the Ni d -states. This many-pole self-energy includes a more realistic treatment of inelastic losses than the plasmon pole model, and yields improved agreement with experiment, as seen from Fig. 6(b). These results demonstrate that an accurate treatment of the delocalized s - p -states can also be important in such systems. Thus in order to achieve good agreement between theoretical and experimental spectral features, a systematic consideration of excited state properties including both localized- and delocalized states seems to be important.

B. LSCO

In recent years, understanding the doping dependence of high T_c cuprates has become an interesting challenge. LSCO ($\text{La}_{2-x}\text{Sr}_x\text{CuO}_4$), which is a prototype of hole-doped cuprates, exhibits metallic and paramagnetic behavior at high doping,¹⁰ and becomes an AF insulator when undoped. Between these limits, the system goes through a superconducting phase at about $x = 0.15$. A good description of the electronic structure in its insulating phase is important to understand the exotic doping dependent phase transformations in such systems.

In the over-doped region with doping concentrations $x > 0.2$, LSCO becomes paramagnetic, and is well described by a self-energy approximation constructed from a single band Hubbard model.¹⁰ A Fermi-liquid description thus becomes more appropriate for such systems. As doping is reduced, correlation effects due to localized states become more important, and the implementation of Hubbard U to the d electrons on the Cu sites is seen to open a gap. A gap correction using GW+ U on the partial d -DOS of Cu and p -DOS of O is shown in Fig. 7. Our O K-edge XAS for GW and GW+ U with $U = 7.0$ eV are compared with experimental results in Fig. 9. Our result agrees qualitatively with the undoped LSCO experiment, while the over-doped LSCO system is adequately reproduced by a GW calculation alone ($U = 0$). This result is not surprising, since in the absence of the Hubbard term, the LDA does not predict a correlation gap. As a result the system is predicted to be metallic, mimicking the over-doped ($x \approx 0.3$) paramagnetic phase of

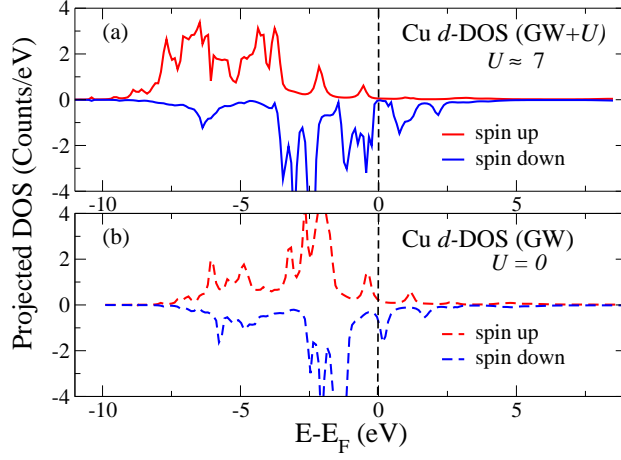


FIG. 7: (Color online) (a) GW+ U ($U=7.5$ eV) Cu spin up (solid red) and down (dashed blue) d -DOS; (b) GW ($U=0.0$) Cu spin up and down d -DOS. The vertical dashed line is at the Fermi energy.

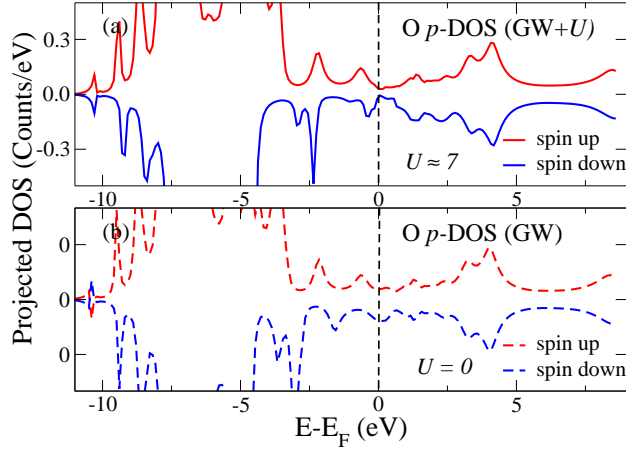


FIG. 8: (Color online) (a) GW+ U ($U=7.0$ eV) O spin up (solid red) and down (dashed blue) p -DOS; (b) GW ($U=0.0$) O spin up and down p -DOS. The vertical dashed line is at the Fermi energy.

$\text{La}_{1-x}\text{Sr}_x\text{CuO}_4$. A complete description of the doping dependence of spectral features from over-doped ($x = 0.3$) to undoped ($x = 0.0$), requires a dynamical self-energy correction that incorporates pseudo-gap, superconducting, and Fermi-liquid physics.⁴¹

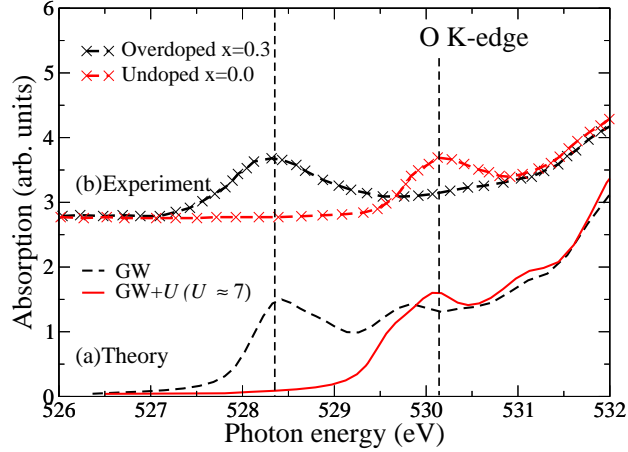


FIG. 9: (Color online) O K-edge XAS for LSCO: (a) our GW+ U calculation with for $U = 7.0$ (red) and GW only (black); (b) experimental K-edge XAS for undoped ($x = 0.0$, red) and over-doped ($x = 0.3$, black) LSCO, and the vertical dashed lines are a guide to the eye.

IV. SUMMARY AND CONCLUSIONS

We have implemented a Hubbard model adapted from the LSDA+ U method of Anisimov *et al.* as an extension of the real-space Green's function approach for calculations of x-ray spectra of correlated materials. In our construction two parameters U and J are chosen to match the experimental gap. These Hubbard parameters are introduced in terms of an effective self-energy correction leading to a GW+ U approach which provides an efficient way to account for local correlation effects on x-ray spectra. Such a theoretical understanding of O K-edge XAS and XES is useful to explain key electronic features of strongly correlated systems. For example, in the AF insulating phases of transition metal oxides, several important features of the experimental profile of the O K-edge XAS and XES, and in particular the correlation-gap, require theoretical treatments beyond the quasi-particle approximation.

Our GW+ U approach yields results which are in good agreement with experiment for the O K-edge spectrum of MnO and NiO. However, the agreement is only qualitative for more complex systems such as LSCO. This suggests the need for including a more comprehensive treatment of superconducting and pseudo-gap physics capable of incorporating doping dependence in the under-doped regime of such systems.^{41,42} Finally we note that our current approach is limited to the quasi-particle approximation together with Hubbard

model corrections, while many-body effects such as satellites are neglected. However, some of these many-body aspects can be obtained by incorporating additional charge transfer contributions in the Hamiltonian.^{43,44}

V. ACKNOWLEDGMENT

We thank A. Bansil and R. Markiewicz and especially P. Rinke for stimulating suggestions. This work is supported by the Division of Materials Science & Engineering, Basic Energy Sciences, US Department of Energy Grants DE-FG03-97ER45623 and DE-FG02-07ER46352. This research also benefited from the collaboration supported by the Computational Materials Science Network (CMSN) program of US DOE under grant DE-FG02-08ER46540.

-
- ¹ G. Onida, L. Reining, and A. Rubio, *Rev. Mod. Phys.* **74**, 601 (2002).
 - ² L. Hedin and S. Lundqvist, *Solid State Phys.* **23**, 1 (1969).
 - ³ V. I. Anisimov, J. Zaanen, and O. K. Andersen, *Phys. Rev. B* **44**, 943 (1991).
 - ⁴ V. I. Anisimov, F. Aryasetiawan, and A. I. Lichtenstein, *J. Phys.: Condens. Matter* **9**, 767 (1997).
 - ⁵ H. Jiang, R. I. Gomez-Abal, P. Rinke, and M. Scheffler, *Phys. Rev. B* **82**, 045108 (2010).
 - ⁶ H. Jiang, R. I. Gomez-Abal, P. Rinke, and M. Scheffler, *Phys. Rev. Lett.* **102**, 126403 (2009).
 - ⁷ T. Das, R. S. Markiewicz, and A. Bansil, *Phys. Rev. B* **81**, 174504 (2010).
 - ⁸ R. S. Markiewicz, S. Sahrakorpi, and A. Bansil, *Phys. Rev. B* **76**, 174514 (2007).
 - ⁹ S. Basak, T. Das, H. Lin, J. Nieminen, M. Lindroos, R. S. Markiewicz, and A. Bansil, *Phys. Rev. B* **80**, 214520 (2009).
 - ¹⁰ T. Ahmed, T. Das, J. J. Kas, H. Lin, R. S. Markiewicz, A. Bansil, J. J. Rehr, B. Barbiellini, and F. D. Vila (2011), in Press.
 - ¹¹ J. J. Kas, A. P. Sorini, M. P. Prange, L. W. Cambell, J. A. Soininen, and J. J. Rehr, *Phys. Rev. B* **76**, 195116 (pages 10) (2007).
 - ¹² O. Bengone, M. Alouani, P. Blöchl, and J. Hugel, *Phys. Rev. B* **62**, 16392 (2000).
 - ¹³ H. Ebert, A. Perlov, and S. Mankovsky, *Solid State Communications* **127**, 443 (2003).

- ¹⁴ P. Krüger, Journal of Physics: Conference Series **190**, 012006 (2009).
- ¹⁵ E. Z. Kurmaev, R. G. Wilks, A. Moewes, L. D. Finkelstein, S. N. Shamin, and J. Kuneš, Phys. Rev. B **77**, 165127 (2008).
- ¹⁶ J. J. Rehr, J. J. Kas, F. D. Vila, M. P. Prange, and K. Jorissen, Phys. Chem. Chem. Phys. **12**, 5503 (2010).
- ¹⁷ J. J. Rehr, J. J. Kas, M. P. Prange, A. P. Sorini, Y. Takimoto, and F. Vila, Comptes Rendus Physique **10**, 548 (2009).
- ¹⁸ A. Ankudinov and J. Rehr, Phys. Rev. B **62**, 2437 (2000).
- ¹⁹ U. von Barth and L. Hedin, J. Phys. C: Solid State Phys. **5**, 1629 (1972).
- ²⁰ A. Ankudinov, B. Ravel, J. Rehr, , and S. Conradson, Phys. Rev. B **58**, 7565 (1998).
- ²¹ J. J. Rehr and R. C. Albers, Rev. Mod. Phys. **72**, 621 (2000).
- ²² W. von der Linden and P. Horsch, Phys. Rev. B **37**, 8351 (1988).
- ²³ A. Georges, AIP Conference Proceedings **715**, 3 (2004).
- ²⁴ R. C. Albers, N. E. Christensen, and A. Svane, J. Phys.: Condens. Matter **21**, 343201 (2009).
- ²⁵ O. Gunnarsson, O. K. Andersen, O. Jepsen, and J. Zaanen, Phys. Rev. B **39**, 1708 (1989).
- ²⁶ I. V. Solovyev and M. Imada, Phys. Rev. B **71**, 045103 (2005).
- ²⁷ F. Aryasetiawan, K. Karlsson, O. Jepsen, and U. Schönberger, Phys. Rev. B **74**, 125106 (2006).
- ²⁸ M. Cococcioni and S. de Gironcoli, Phys. Rev. B **71**, 035105 (2005).
- ²⁹ V. I. Anisimov, I. V. Solovyev, M. A. Korotin, M. T. Czyżyk, and G. A. Sawatzky, Phys. Rev. B **48**, 16929 (1993).
- ³⁰ B. Fromme, *Electronic Structure of MnO, CoO, and NiO*, vol. 170 of *Springer Tracts in Modern Physics* (Springer Berlin Heidelberg, 2001).
- ³¹ S. Liu and W. Langenaeker, Theoretical Chemistry Accounts: Theory, Computation, and Modeling (Theoretica Chimica Acta) **110**, 338 (2003).
- ³² F. Aryasetiawan, K. Karlsson, O. Jepsen, and U. Schönberger, Phys. Rev. B **74**, 125106 (2006).
- ³³ J. P. Perdew, R. G. Parr, M. Levy, and J. L. Balduz, Phys. Rev. Lett. **49**, 1691 (1982).
- ³⁴ A. E. Berkowitz and K. Takano, Journal of Magnetism and Magnetic Materials **200**, 552 (1999).
- ³⁵ B. Morosin, Phys. Rev. B **1**, 236 (1970).
- ³⁶ K. Nakahigashi, N. Fukuoka, and Y. Shimomura, J. Phys. Soc. Jpn. **38**, 1634 (1975).
- ³⁷ H. Kondoh and T. Takeda, J. Phys. Soc. Jpn. **19**, 2041 (1964).
- ³⁸ L. V. Dobysheva, P. L. Potapov, and D. Schryvers, Phys. Rev. B **69**, 184404 (2004).

- ³⁹ H. Kurata, E. Lefèvre, C. Colliex, and R. Brydson, Phys. Rev. B **47**, 13763 (1993).
- ⁴⁰ T. Kotani and M. van Schilfgaarde, J. Phys.: Condens. Matter **20**, 295214 (2008).
- ⁴¹ R. S. Markiewicz, T. Das, and A. Bansil, Phys. Rev. B **82**, 224501 (2010).
- ⁴² T. Das, R. S. Markiewicz, and A. Bansil, Phys. Rev. B **81**, 174504 (2010).
- ⁴³ L. Hedin, J. Phys.: Condens. Matter **11**, R489 (1999).
- ⁴⁴ J. D. Lee, O. Gunnarsson, and L. Hedin, Phys. Rev. B **60**, 8034 (1999).